PERGAMON

Journal of Structural Geology 24 (2002) 1215–1231

JOURNAL OF STRUCTURAL GEOLOGY

www.elsevier.com/locate/jstrugeo

Progressive localisation of strain during the evolution of a normal fault population

V. Meyer[a,b], A. Nicol[a,c], C. Childs[a,*], J.J. Walsh[a], J. Watterson[a,d]

[a]*Fault Analysis Group, Department of Geology, University College Dublin, Belfield, Dublin 4, Ireland*
[b]*Université de Nice Sophia-Antipolis, UMR Géosciences Azur, Les Lucioles 1, Batiment 4, 250 Rue Albert Einstein, 06560 Valbonne, France*
[c]*Institute of Geological and Nuclear Sciences, PO Box 30368, Lower Hutt, New Zealand*
[d]*Fault Analysis Group, Liverpool University Marine Laboratory, Port Erin, Isle of Man IM9 6JA, UK*

Received 28 November 2000; revised 2 February 2001; accepted 8 August 2001

Abstract

The evolution of a syn-sedimentary normal fault population has been established from the analysis of a high-quality 3D seismic reflection survey from the Timor Sea, offshore NW Australia. Growth of the fault population, which initiated ca. 6 Ma ago, occurred in three distinct but temporally overlapping stages. The initial stage of fault population evolution was characterised by rapid growth of fault length in the first 1–2 Ma of extension. Displacement rates of individual faults were established during this stage and were constant throughout subsequent fault growth. The second stage involved amplification of fault displacements on existing fault traces with minimal fault propagation. During the third stage, shortening of the traces of active faults and high mortality rates for small faults resulted in a net decrease in fault trace length on successively younger horizons. This stage was accompanied by a declining extension rate.

Fault throw populations have constant slopes on each syn-faulting horizon; however an up-sequence shallowing of the slope of length and geometric moment populations demonstrates a progressive concentration of strain onto fewer and larger faults through time. If extension were to continue beyond the present value of 4.5%, this strain localisation might culminate in the formation of a single active through-going fault.

Keywords: Normal fault population; Fault growth; Displacement rate; Strain localisation

1. Introduction

Studies of ancient normal fault systems indicate that faults grow by increases in cumulative displacement and fault length through time (e.g. Watterson, 1986; Walsh and Watterson, 1988; Marrett and Allmendinger, 1991; Cowie and Scholz, 1992; Gillespie et al., 1992; Dawers et al., 1993; Schlische et al., 1996). Geometrical and kinematic analysis of fault populations (Walsh and Watterson, 1991; Anders and Schlische, 1994; Peacock and Sanderson, 1994; Cartwright et al., 1995; Childs et al., 1995; Dawers and Anders, 1995; Nicol et al., 1997; Ferrill et al., 1999; Walsh et al., 2001) together with numerical (e.g. Cowie et al., 1993; Cowie, 1998; Gupta and Scholz, 2000) and physical modelling (McClay, 1990; Childs et al., 1993; Meyer, 1997; Marchal et al., 1998; Ackermann et al., 2001), indicate that faults increase in both displacement and length through time and that fault systems become more linked with increasing finite strains. Few geological datasets, however, enable the temporal evolution of fault populations to be established, and key questions remain concerning fault growth through time. For example, do fault lengths and maximum displacements increase at rates which are constant during the lifetime of a fault, or are there times when fault dimension increases more rapidly than displacement? Do all faults within a given population evolve in a similar manner independent of size? And does strain within a fault array become concentrated on the largest faults over a geological timescale?

These questions are best resolved by detailed analysis of syn-sedimentary fault systems where changes in sequence thicknesses across faults record fault displacements through time (Childs et al., 1993; Clausen et al., 1994; Nicol et al., 1997). Such analyses require that sedimentation rates outstrip displacement rates and that little or no material has been eroded from the footwalls of faults; this condition is most likely to occur for small to moderate sized faults. Where ages are available for syn-faulting horizons, absolute rates of growth of individual faults and fault populations can

* Corresponding author. Fax: +353-1-706-2607.
E-mail address: conrad@fag.ucd.ie (C. Childs).

0191-8141/02/$ - see front matter
PII: S0191-8141(01)00104-3

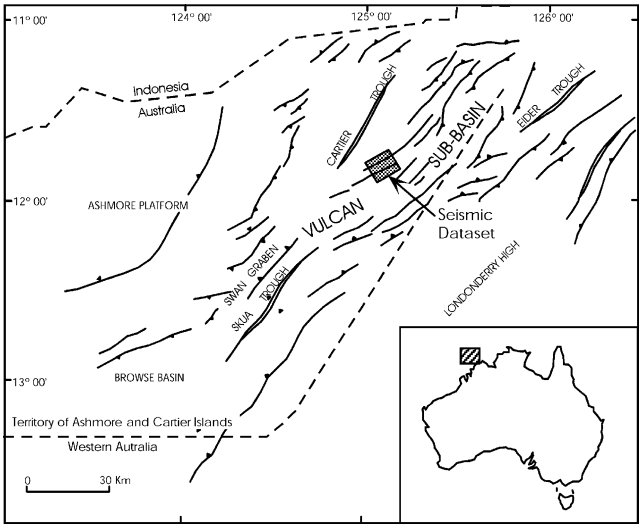

Fig. 1. Location map of the study area (after Wormald, 1988).

be determined. Each of these conditions is satisfied in the Timor Sea study area and here we chart the growth of small to moderate sized normal faults (maximum displacements 2–180 m) over six intervals of time from a high quality seismic reflection dataset. The evolution of the fault trace length and displacement populations for all of the resolvable faults is described from the initiation to cessation of faulting, providing insights into evolution of a normal fault population and identifying the principal factors that influence fault growth in the study area.

1.1. The study area

The study area is located in the Vulcan Sub-basin of the Timor Sea, at the northern edge of the Australian northwest continental margin (Fig. 1). The Vulcan Sub-basin is a predominantly NE-trending rift characterised by en échelon normal faults (Woods, 1992), which bound tilted fault blocks in the south and form conjugate structures in the north. The Vulcan Sub-basin has been subjected to two phases of extension; an initial NW–SE directed extension during the Late Jurassic–Early Cretaceous which terminated at an Intra-Valangian Disconformity (Fig. 2a)

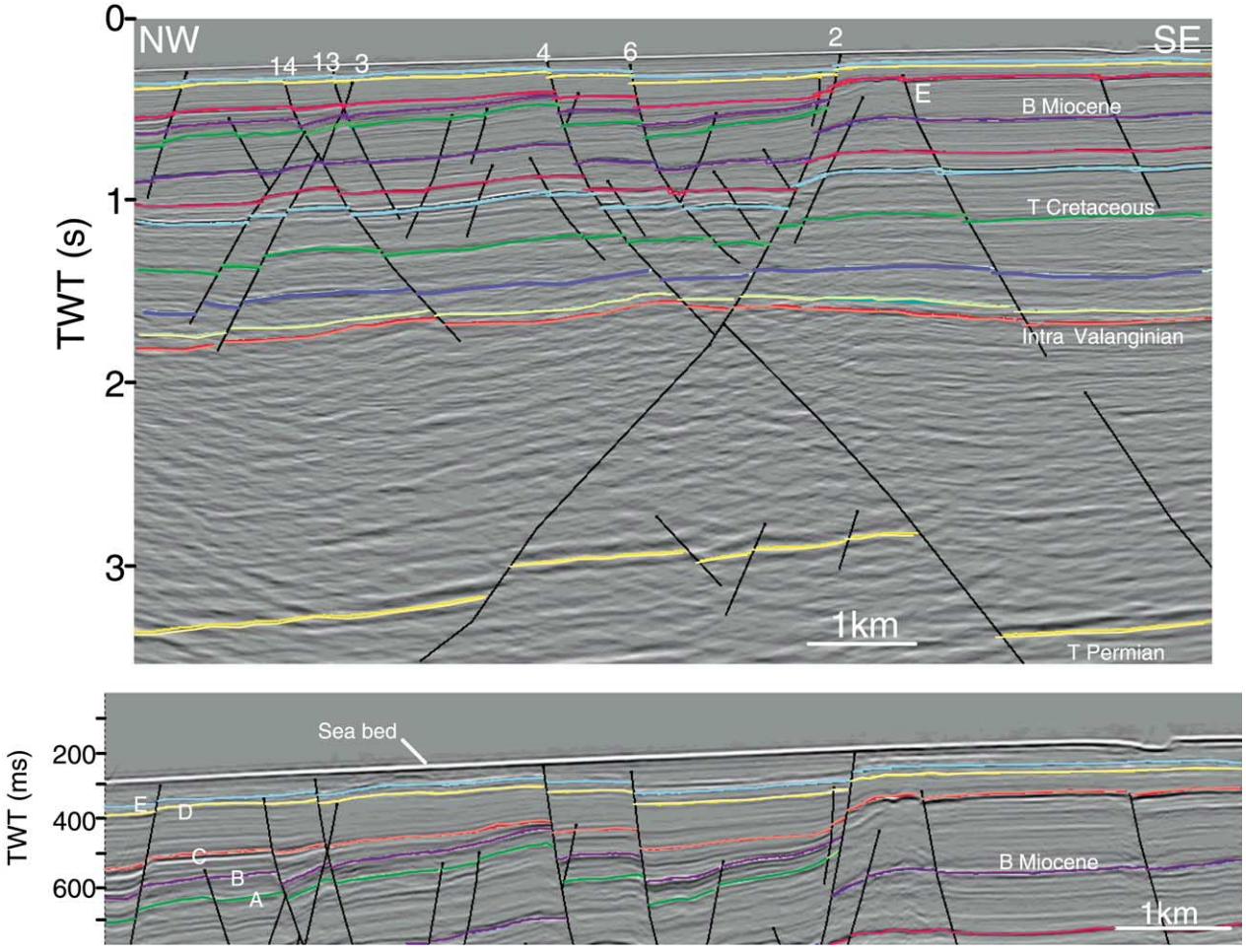

Fig. 2. (a) Representative seismic dip-line showing the 13 interpreted horizons and faults. (b) Enlargement of the upper 800 ms of (a). Horizons A to E are within the syn-faulting sequence.

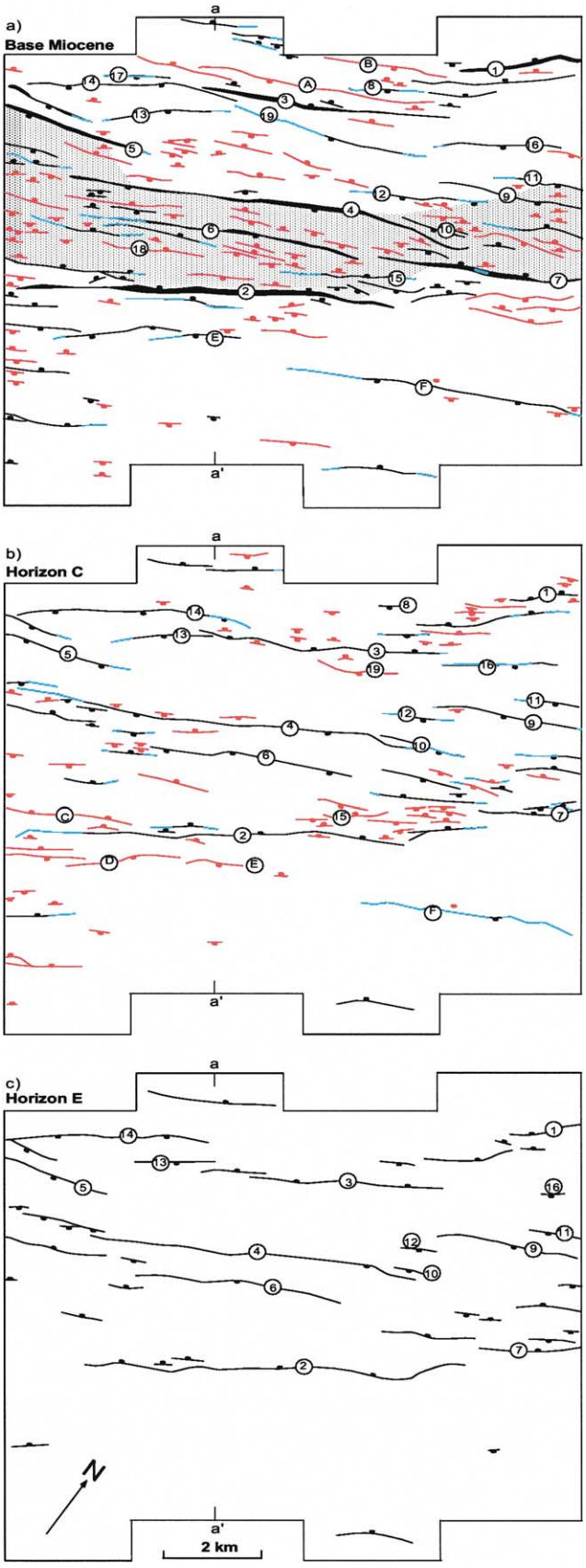

followed by near parallel Tertiary extension (O'Brien et al., 1993; O'Brien and Higgins, 1996). A significant upper Miocene erosional event pre-dates Tertiary faulting within the study area (Pattillo and Nicholls, 1990; Woods, 1992).

The study area comprises NE-striking normal faults which dip at ca. 50–80° NW and SE in approximately equal numbers (Figs. 2 and 3). Faults displace up to eight reflectors by as much as 180 m in a well-imaged 1–1.5-km-thick Cenozoic sequence, which is dominated by shelf carbonates (Pattillo and Nicholls, 1990), and offset a further four reflectors in a poorly imaged underlying Mesozoic sequence. Within the mainly Pliocene and Pleistocene syn-faulting sequence, strata thicken up to 30% across faults with, in some cases, the faults extending to the sea bed.

Tertiary faulting is dominated by a central graben (stippled in Fig. 3a) bounded by two relatively large opposed-dipping faults, which are rooted in Late Jurassic–Early Cretaceous normal faults and form a large conjugate structure (Fig. 2a). These large Tertiary faults originated by reactivation and upward propagation of Mesozoic structures from which they inherited their general strike (Woods, 1992). The spatial pattern of pre-existing Mesozoic structures also partly controls the areal distribution of Tertiary faulting which, on horizons deposited before the onset of extension, is concentrated within, and NW of, the central graben (e.g. Fig. 2a). The majority of faults within the Tertiary sequence do not appear to extend beneath the Intra-Valangian Disconformity. It is not clear whether the limited vertical extent of some faults is due to poor seismic definition beneath the Intra-Valangian but many of the faults show downward decreasing displacements and most likely do not extend down to the well defined Top Permian reflection (Fig. 2a). Faults which displace the Top Permian (Fig. 2) mainly dip to the SE and during the initial stages of Tertiary faulting SE dipping faults also dominated. Only during Tertiary extension did NW dipping faults begin to accommodate significant basinal displacements.

On pre-faulting Tertiary horizons, fault trace lengths range up to ca. 8.2 km and at least 95% of faults have high lateral tip-line displacement gradients characteristic of fault interaction (Nicol et al., 1996). Thus relay zones between adjacent synthetic faults are common, particularly in the older syn-faulting and younger pre-faulting sequences. On shallower, and therefore younger horizons, the number of faults progressively decreases and only about one third of the faults on the Base Miocene intersect the uppermost mapped horizon (Horizon E) (compare Fig. 3a–c; Table 1).

Fig. 3. Fault maps of (a) pre-faulting Base Miocene, (b) Horizon C and (c) Horizon E illustrating the change in fault pattern through time. Fault traces shown red on (a) and (b) are those which became inactive prior to Horizon C and between Horizons C and E, respectively. Parts of fault traces shown blue indicate retreating tip-lines over the same intervals. Faults numbered 1 to 19 are the same as those labelled in Fig. 4. Faults labelled A to F are referred to in the text.

Table 1
General characteristics of the five syn-sedimentary horizons

Horizon	Age (Ma)	No. faults	Max throw (m)	Max fault length (km)	Av. extension (%)
A	6 (±0.5)	91	174	8.2	4.4
B	4.7 (±0.5)	79	149	8.2	2.8
C	2.7 (±0.5)	65	105	7.8	1.2
D	1.8 (±0.3)	39	78	7.3	0.6
E	1.3 (±0.3)	35	63	7.3	0.4

1.2. Data

The data are derived from a high quality 3D seismic reflection survey covering a $12 \times 11.3\ km^2$ area and comprising 483 NW/SE trending inlines and 902 crosslines spaced at 25 and 12.5 m, respectively. The seismic data extend to 5 s two-way travel time (TWT). Thirteen horizons, ranging in age from Permian to Pleistocene, have been interpreted on every 10th inline over the survey area and locally every single or 5th line. Five of the interpreted horizons are within the syn-faulting Tertiary sequence.

The five interpreted syn-faulting horizons, labelled A to E, range in age from ca. 6 to 1.3 Ma (Table 1). There are no wells within the study area, but ages for the interpreted horizons have been determined by tying the seismic picks in the 3D seismic survey to an overlapping regional 2D survey that covers both a published seismic line (Woods, 1992) and the Oliver-1 well 12 km to the west of the study area. Woods provides seismic picks for the Base Pliocene (5.3 Ma), Top Early Pliocene (3.6 Ma) and Top Pliocene (1.8 Ma). Horizon D in this study is the Top Pliocene and the ages of the four additional syn-faulting seismic picks have been calculated from the three dated reflectors assuming a constant sedimentation rate during the period of fault activity. Although the age data are not sufficient to test this assumption, averaged sedimentation rates in the Early and Late Pliocene are approximately equal (within 20%) in the Oliver-1 well. Uncertainties in ages due to the assumption of constant sedimentation rate are reflected in the error ranges attached to the horizon ages (Table 1). Horizons C–E extend over the entire map area, while A and B are eroded to the SE of the main region of faulting. Seismic velocities determined from wells adjacent to the study area have been used to depth convert fault throws within the study area.

2. Fault displacements and bulk extension

Evidence for growth of the fault population is preserved in the patterns of displacement variation on fault surfaces within the syn-faulting sequence. Here vertical displacements, or fault throws, were recorded as differences in TWT between footwall and hanging wall cutoffs and have been converted to depth using a velocity of $2400\ ms^{-1}$ (i.e. 1 ms TWT = 1.2 m) for the syn-faulting sequence; within the pre-faulting sequence seismic velocities are in excess of $3000\ ms^{-1}$. The TWT/distance relationship within the syn-faulting sequence is not strictly linear and we estimate, from seismic velocities measured in wells in adjacent areas that velocity variations could result in an error of up to ±5% in throw values, an acceptable precision for analysis of displacements. Detailed displacement analysis has been confined to faults in the upper part of the faulted sequence where faulting and sedimentation were synchronous and seismic data quality is highest.

Vertical profiles of present day throw against horizon age for 20 faults are presented in Fig. 4. The profiles are from seismic dip lines that pass through the point of maximum displacement on each fault surface. These profiles include all faults with maximum throws >85 m within the syn-faulting sequence in addition to about 50% of all faults with maximum throws of 30–85 m. The profiles in general have maximum throw values on Horizon A (Fig. 4a). Downward decrease in throw below the point of maximum throw is relatively gradual with low displacement gradients ($\ll 0.1$) typical of blind faults. Displacement decreases rapidly above the point of maximum displacement. The high displacement gradients (>0.1) above Horizon A, are characteristic of syn-sedimentary faults where progressively younger horizons record less of the displacement history of the growing fault. Because there is no erosion on the footwalls of these faults, the difference in throw between two successive syn-faulting horizons is the throw that accumulated on the fault in the time interval between deposition of the two horizons. The gradient measured between successive points on a profile of throw against horizon age is therefore the average fault displacement rate over the relevant time interval (Fig. 4b).

For about one quarter of the faults in Fig. 4b, throws are approximately equal on Horizons A and B and a marked change in profile gradient defining the onset of faulting (cf. Childs et al., 1993), occurs at Horizon B. The remaining faults initiated either at Horizon A or between deposition of Horizons A and B. For occasional faults, e.g. Fault 7, extrapolated throw gradients within the pre- and syn-faulting parts of the throw profile intersect at a point below Horizon A suggesting that these faults may have initiated immediately prior to deposition of Horizon A.

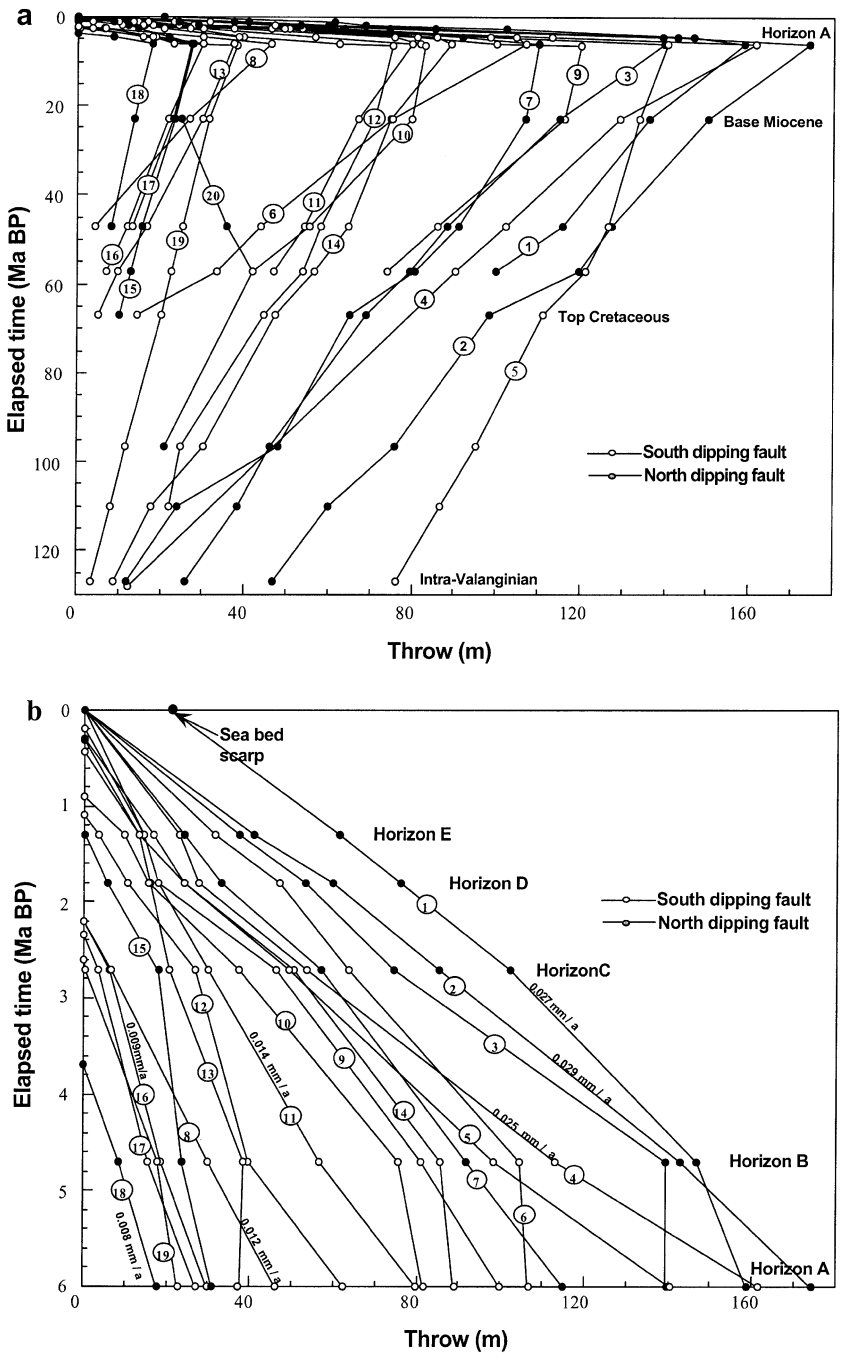

Fig. 4. (a) Throw versus horizon age profiles for 20 large faults within the study area. (b) Enlargement of the upper part of (a) showing only the syn-faulting sequence. The locations of the faults labelled 1–20 are shown in Fig. 3. Filled circles indicate North-dipping faults and open circles are South-dipping faults. Selected fault throw rates are provided for reference (mm y^{-1}). One fault offsets the sea-bed.

Therefore all of the faults in Fig. 4b commenced growth during the period immediately prior to deposition of Horizon A to deposition of Horizon B, i.e. the first 1–2 my of extension.

Changes in slope of the throw vs. horizon age profile between mapped horizons reflect changes in fault displacement rate through time (Childs et al., 1993; Nicol et al., 1997). From the initiation of fault growth, displacement rates were near constant for individual faults but varied with fault size (Fig. 4b). Larger faults, with larger than average cumulative displacements and fault lengths, were always characterised by higher displacement rates than smaller faults. This hierarchy of fault size and related behaviour was established relatively early in the

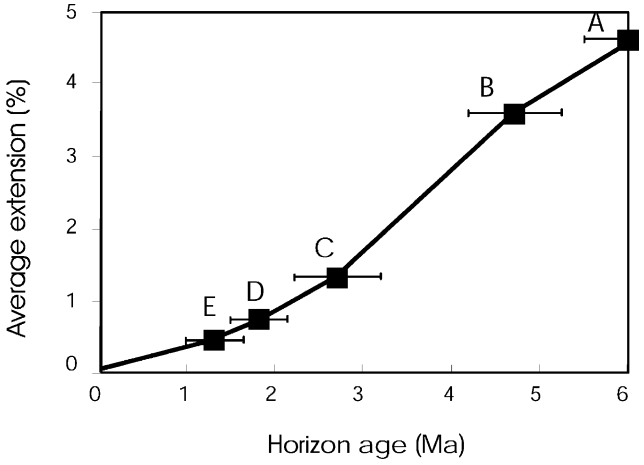

Fig. 5. Plot of extension vs. horizon age for the five syn-faulting horizons.

development of the system (Nicol et al., 1997). Displacement rates on individual faults vary between ca. 0.008 and 0.03 mm a^{-1} and are towards the lower end of the range of displacement rates recorded on similar syn-sedimentary faults in other normal fault systems (Nicol et al., 1997).

The stratigraphic position of the upper tip-point of a syn-sedimentary fault indicates the time at which fault movement ceased. On a throw vs. horizon age profile (Fig. 4b) the timing of fault death is provided by the intercept with the elapsed time axis. All but one fault with maximum cumulative throws >90 m on Horizon A intersect the sea-bed reflector. Only in one case does the rate of fault displacement exceed the rate of deposition or erosion to form a sea-bed scarp. By contrast, all faults with maximum cumulative displacements of <90 m on Horizon A are now inactive with individual faults dying mainly between deposition of Horizon C and the present. Fault mortality rate is therefore correlated with maximum cumulative fault displacement. Large displacement structures did not however become large merely because they outgrew their smaller and shorter lived neighbours. Higher displacement rates are characteristic of large faults throughout their growth such that currently larger faults were also larger and moving faster than average throughout the growth of the fault system (Nicol et al., 1997).

Given the high mortality rates for smaller faults and the near-constant displacement rates on individual faults, it might be expected that rates of bulk extension across the map area decreased over the last 1–2 Ma. A plot of extension, calculated from the cumulative heaves of all faults and averaged over 99 fault-normal seismic lines, against time (Table 1; Fig. 5), suggests that such a reduction in the number of faults, particularly above Horizon E, is linked in part to this decrease in extension rate. The death of small faults is not however entirely attributable to decreasing extension rate, since at earlier stages of fault system evolution (pre-Horizon C) extension rates were approximately constant and smaller faults were already dying.

The calculation of fault-displacement rates from throw vs. horizon age profiles (Fig. 4b) assumes that upward decreases in displacement within the syn-faulting sequence reflect only the growth history of faults and associated syn-depositional thickness changes at the contemporaneous free surface. However, vertical displacement gradients within the syn-faulting sequence will also comprise a post-depositional component. These post-depositional gradients are accommodated by strains in the rock volume and are equivalent to displacement gradients observed on blind faults. For blind, isolated normal faults, the maximum vertical displacement gradient is ca. 0.1 (Walsh and Watterson, 1989), with mean values at least an order of magnitude lower. Displacement gradient magnitudes depend on lithology and degree of lithification of the faulted sequence. The shelf carbonate sequence above the Base A in the Timor Sea is likely to have become lithified relatively quickly and is therefore unlikely to sustain high post-depositional displacement gradients. However, if we assume that post-depositional gradients in the Timor Sea area may be as high as 0.1, equivalent to a 30 m decrease in throw over the 300 m mean depth interval between Horizons A and E, then the apparent displacement rate due to post-depositional displacement gradients is 0.006 mm a^{-1}. Therefore small faults (throw <30 m) with estimated displacement rates less than 0.006 mm a^{-1} could be entirely post-depositional and displacement gradients on larger faults may be overestimated by up to 0.006 mm a^{-1}. If we assume a more realistic vertical throw gradient of 0.01 then overestimates of displacement rate are reduced by an order of magnitude.

A more direct estimate of the likely magnitude of post-depositional gradients is provided by comparing the change in displacement gradients above and below Horizon B for those faults that initiated after deposition of this horizon. The occurrence of near zero gradients on, for example, Faults 3, 6, 13 and 14 below Horizon B (Fig. 4b) suggests that in the absence of free surface interaction, post-depositional gradients within the syn-faulting sequence are far lower than 0.1. We conclude that post-depositional gradients are likely to be negligible but in the extreme case could be responsible for a 0.006 mm a^{-1} overestimate of displacement rate, an error which is insignificant in the context of this article.

3. Changes in fault populations through time

One means of quantifying changes in a fault system as strain accumulates is to analyse the distribution of fault-sizes at several points in time. Here we use log–log cumulative-frequency plots to analyse 2D maximum-throw, fault length and geometric-moment populations sampled from the five horizons within the syn-faulting

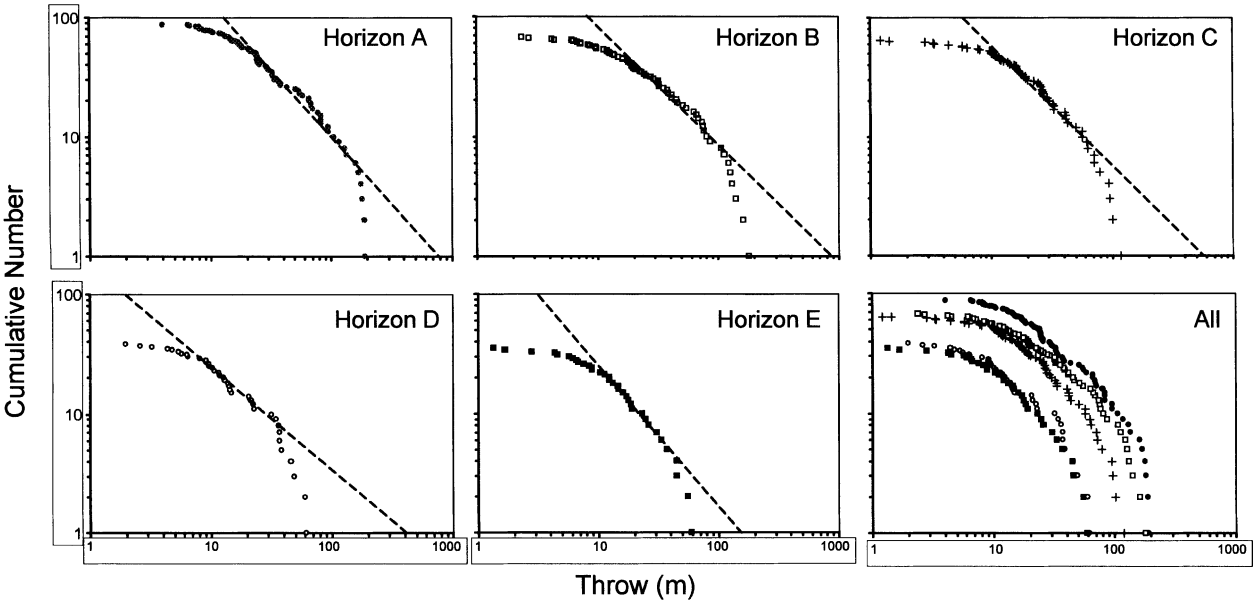

Fig. 6. Maximum displacement 2D cumulative frequency plots for the five syn-faulting horizons A–E. The dashed lines are best fit lines through the straight portions of the population curves; the slopes of the best fit lines are given in Table 2.

sequence. Fault populations from seismic datasets typically apply to a limited size range determined at the lower bound by the effective limit of seismic resolution and at the upper bound by the largest fault in the sample area (Walsh and Watterson, 1991; Yielding et al., 1992). Curves generally define a straight-line segment over at least 1–1.5 orders of magnitude describing a scale invariant, or power-law, distribution (Childs et al., 1990; Heffer and Bevan, 1990; Marrett and Allmendinger, 1990, 1992; Walsh et al., 1991; Yielding et al., 1992), but exponential fault size populations have also been recorded (e.g. Clifton et al., 2000). Here we are primarily concerned with identifying changes in the fault size distribution through time and although a number of the curves approximate to power-law distributions, the precise form of these distributions is not critical for comparative purposes. The fault-size populations of fault trace length and maximum displacement were extracted from a series of maps such as those shown in Fig. 3. Horizons A and B are absent in the relatively unfaulted region to the SE of the central graben (Fig. 3). In this region six faults on Horizon A and 15 faults on Horizon B were either partly, or entirely, eroded and for these faults, sizes were estimated by calculating the average of values from the Base Miocene and Horizon C. Small displacement (<ca. 10 m) faults identified on only one seismic line are shown on Fig. 3, but do not yield a fault length and are therefore not included in the 2D size populations.

3.1. Fault-trace maximum displacement

Cumulative frequency curves of maximum throw are characterised by a left-hand section of low slope, a central segment of intermediate slope which approximates to a straight-line and a steep right-hand tail (Fig. 6). The lower limit of the central segments of all curves occurs at throws of 9–14 m and marks the effective limit of seismic resolution for fault throw; throws less than ca. 10 m are not adequately sampled. The main differences between population curves are that the largest fault size and the total number of faults decrease by similar proportions up-sequence. The main cause of these differences is that younger horizons record less of the fault system evolutionary trend characterised by

Table 2
Population slopes of maximum throw (E_D) and length of the five syn-sedimentary horizons. Slopes for the fault length populations have been determined both from the raw data (E_L) and modified populations (ELM) which have been corrected for fault truncation (see text). Slopes of displacement vs. length were derived from the throw and length populations (E_L/E_D) and from cross-plots of throw and length for each horizon (D vs. L)

Horizon	Max. throw (E_D)	Trace length (E_L)	Trace length (ELM)	E_L/E_D	D vs. L
A	− 1.06	− 1.61	− 1.78	1.68	1.93
B	− 0.99	− 1.46	− 1.77	1.79	2.10
C	− 1.00	− 1.41	− 1.57	1.57	2.37
D	− 0.85	− 1.05	− 1.21	1.42	1.35
E	− 1.15	− 1.05	− 1.20	1.04	1.39

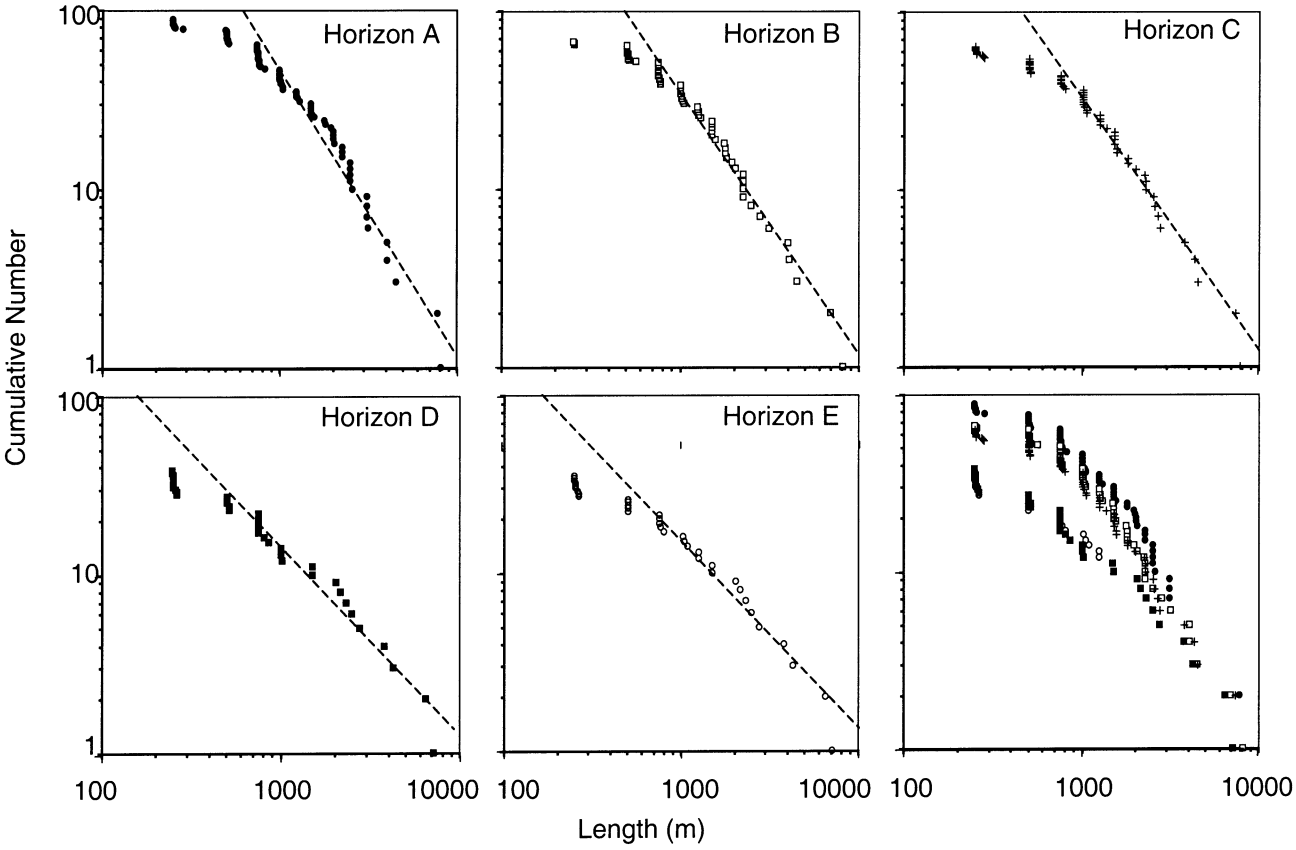

Fig. 7. Fault length cumulative frequency plot for the five syn-faulting horizons. The dashed lines are best fit lines through the straight portions of the population curves; the slopes of the best fit lines are given in Table 2.

a progressive decrease in the number of active faults. Fault mortality rates decrease with fault size and few of the small faults (e.g. <20 m) on the Base Miocene horizon (red trace Fig. 3a), for example, remained active at Horizon E (Fig. 3c). The net effect is a bulk shift of the curves towards the *y*-axis for progressively younger horizons and a reduction in the length of the central straight-line segment from ca. 1 to 0.5 orders of magnitude (Fig. 6 Horizon A and E). The slope of the straight line segment remains about −1 on all syn-faulting horizons (Table 2), although the precision of the measured slope degrades up-sequence.

The throw populations in Fig. 6 are for the present-day cumulative throws on the mapped horizons rather than for the active fault populations at the time of deposition of each horizon. However, the slope of each throw population is approximately the same for each horizon irrespective of whether it records the entire fault growth history (Horizon A) or only the last 1 my of fault system evolution (Horizon E). This condition can only arise if the slope of the active fault population is approximately constant through time and we conclude that the fault throw population slope has not changed significantly during the evolution of the fault system.

The tail on the right-hand side of the maximum throw population curves are largely due to segmentation of the traces of the largest faults in the area. The largest faults do not extend across the entire map but are arranged into en échelon patterns with transfer of displacement between the fault segments via relay zones (e.g. Faults 4 and 9 or Faults 2 and 7; Fig. 3). The tail in the population distribution could be largely removed by treating each segmented fault array as a single structure. If this approach were taken, however, then the increased length of the largest structures would result in a tail on the cumulative length populations, which are discussed below.

3.2. Fault-trace length

Populations of fault trace lengths cover the range from 250 m (sample-line spacing) to 8.2 km and have long straight central segments (ca. one order of magnitude) and short steep right-hand tails (Fig. 7). Fault length data are subject to sampling artefacts in the form of censoring where faults extend outside the sample area and truncation where displacements fall below the effective limit of resolution (Heffer and Bevan, 1990). In addition, measured fault lengths derived from seismic reflection datasets are influenced to a variable degree by the line spacing. The effects of truncation are proportionally more significant on smaller faults (Walsh et al., 1996; Yielding et al., 1996) and in Fig. 7 cause the curves to shallow at lengths of ca. 700–1000 m in a similar manner to the maximum throw

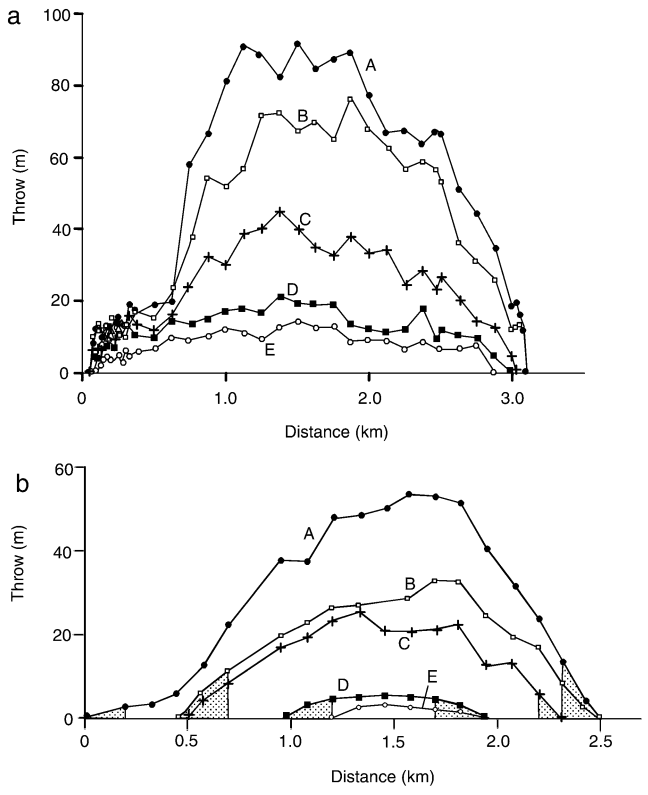

Fig. 8. Throw vs. distance profiles for Horizons A–E on (a) Fault 9 and (b) Fault 12 (see Figs. 3 and 4). Both tips of Fault 12 retreated and the fault shortened from an initial maximum fault length on Horizon A. The right hand tip of Fault 9 retreated slightly while the left hand tip propagated ca. 0.5 km between the times of deposition of Horizons A and E. The stippled areas in (b) indicate the increase in mapped fault trace when the seismic data were interpreted on lines spaced every 25 m rather than 250 m; only selected datapoints in the tip region of this fault are shown.

populations. Censoring also results in the measured fault length being less than the actual value because an unknown length of fault extends outside the sample area. Censoring is likely to have the greatest impact on faults with the largest trace lengths and is not of great significance unless the sample area is small relative to the actual lengths of most of the fault traces (see Heffer and Bevan, 1990; Yielding et al., 1992). In this dataset about 5% of the 2D fault population for each horizon is subject to censoring so that this artefact does not have a significant effect on the populations presented.

The fault trace length populations are characterised by central segments that are approximately straight, albeit with minor steps in some cases, with slopes that decrease up sequence from −1.61 to −1.05 (Fig. 7; Table 2). This change in slope is particularly marked between Horizons C and D and reflects three main controls. Firstly, the lengths of the largest two faults in this study (Faults 2 and 4 in Fig. 3) decrease by only 10–15% (see also Table 1) so that the upper bound on the curves is essentially fixed in log–log space. Secondly, the total number of faults decreases up-sequence, moving the lower boundary of the curve downwards for younger horizons. Thirdly, trace lengths of individual small and medium faults typically diminish up-sequence; for example, compare the lengths of Faults 5, 10, 12 and 16 in Fig. 3b and c. Understanding how much of this reduction in trace length is due to truncation and sample-line spacing, and how much is due to an actual decrease of fault trace lengths on progressively younger horizons is important for interpreting the length populations.

To evaluate the influence of displacement truncation and line spacing on fault trace length, we have examined seismic lines spaced at 25 m in the tip regions of six faults. This dramatically reduces the impact of sample-line spacing and by detailed examination of multiple closely-spaced lines reduces the effective limit of vertical seismic resolution by ca. 50% down to 4–6 m. For those faults where the tips were more precisely located, which include the fault in Fig. 8a, the trace length not sampled at each fault tip for the initial 2D population was typically <250 m and averaged 220 m. The length of under-sampled fault trace is independent of fault size (Watterson et al., 1996) and of sample horizon. In order to assess the impact of throw truncation and sample-line spacing on the length populations we have added 440 m (220 m for each tip) to each fault in Fig. 7 and produced modified length populations (Fig. 9). These corrected length populations are generally straighter with slopes which are 0.1–0.3 steeper than the original populations (Table 2) and clearly indicate a decrease in population slope on the younger horizons. We conclude, therefore, that the up-sequence decrease of population slopes is not accounted for by reduction in fault lengths due to throw truncation or line spacing but is of geological origin.

The up-sequence decrease in length population slope is the result of two main factors. Firstly, many of the faults in the array decrease in trace length on younger horizons. This is the case for the fault in Fig. 8b, where trace length decreases from 2.5 to 0.8 km from the A to E horizons, while many of the faults show a significant decrease in length between mapped horizons (e.g. Faults 5, 10, 12 and 16 in Fig. 3a and c).

Secondly, while faults of relatively short trace length are generally active for less time, this relationship includes scatter and a number of longer faults with lengths of 2–5 km (e.g. Faults A–F in Fig. 3a and b) cease activity before many faults with shorter trace lengths. Removing these relatively large faults from the active fault populations on upper horizons has the effect of decreasing the slope. By contrast death of all faults with lengths below a given value would not decrease the slope but would simply reduce the upper limit of the curve.

To assess the relative contributions of decreases in fault lengths, and fault mortality, a pseudo-length population was created for the D horizon (Fig. 10) by removing those faults from the C population which became inactive between deposition of the C and D horizons (coloured in red in Fig. 3b). The pseudo D population incorporates the death of faults but does not include decreases in fault length. The

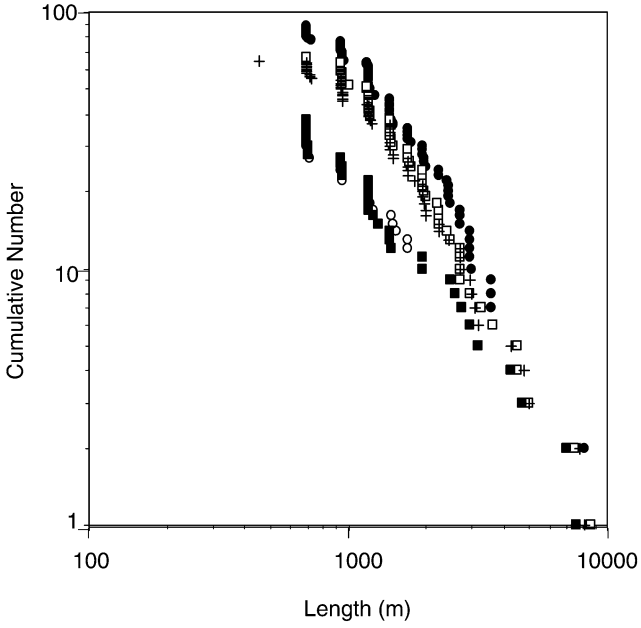

Fig. 9. Fault length cumulative frequency plot for the five syn-faulting horizons corrected for truncation effects (see text). The datapoint symbols are the same as those in Fig. 6.

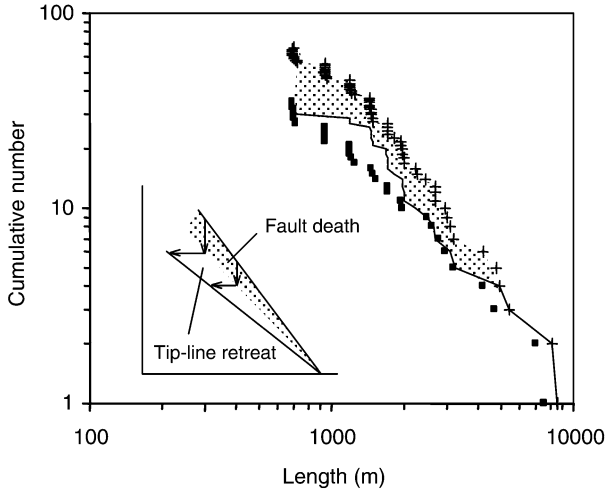

Fig. 10. Fault length cumulative frequency plot for Horizon C (crosses) and Horizon D (filled squares). The difference in slope of the two population curves is due to both a decrease in the numbers of faults, i.e. fault death (see inset) and a decrease in fault length due to tip-line retreat (see inset). The solid line between the Horizon C and D population curves is an intermediate population which excludes faults that died between Horizon C and D times (shaded) but does not include the effect of tip-line retreat.

length populations are those modified for truncation and line-spacing artefacts. The pseudo population has a maximum trace length identical to that of Horizon C but is characterised by a slope intermediate between that of the C and D horizons. The disparity in slopes between the C and pseudo D populations is due entirely to removal of faults within the population, while differences between the D and pseudo D populations are due entirely to decreases in fault lengths. Comparison of the slopes of the C, D and pseudo D populations (Fig. 10) suggests that reduction in fault-trace lengths and cessation of fault movement both contribute to the reduction in population slope between Horizons C and D and are of approximately equal significance. At the largest length values the C and pseudo D populations are the same so that none of the largest faults have become inactive and the difference between the C and D Horizons is due only to decease in fault length. At lower length values there is a variable contribution of fault death and fault length decrease.

We attribute the upward decrease in fault length primarily to a decrease in the lengths of active fault traces through time. An alternative explanation is that the upward decrease in length could be due to the faults having an elliptical upper tip-line centred on the point of maximum displacement on the fault surface, i.e. close to the Base A horizon. In this case successively younger horizons intersect the fault surface along progressively shorter chords. Which of these alternatives is likely to be correct can, for an individual fault, be established from the vertical throw gradients measured between the upper tip-line and the uppermost mapped horizon. Where these gradients are low and within the range expected for blind normal faults (<ca. 0.1) the location of the upper tip-line could be controlled by the overall fault surface shape. Where these gradients exceed those for blind faults, the elevation of the upper tip-line must be controlled by intersection with the contemporaneous free-surface, i.e. that portion of the fault trace became inactive. For some of the larger faults within the study area, vertical throw gradients are as much as 0.5 close to the upper tip-line and the active-trace length of these faults must have decreased through time. For many of the smaller faults the throw on the youngest mapped horizon may be as low as a few metres and vertical throw gradients are within the range expected for blind faults. In these cases it is not possible to determine the cause of shortening of the fault trace. We can therefore be confident that the upward shortening observed on some the larger faults is due to decrease in the active-trace lengths. This cannot be demonstrated for smaller faults, but there are faults with equivalent displacements which have constant trace lengths throughout the syn-faulting sequence.

3.3. Geometric moments

Geometric moment is the product of fault trace length and mean throw. The virtue of analysing geometric moment is that it combines the two most commonly used measures of fault size (i.e. length and displacement) and is a more robust measure than either of these measures in isolation. In addition, geometric

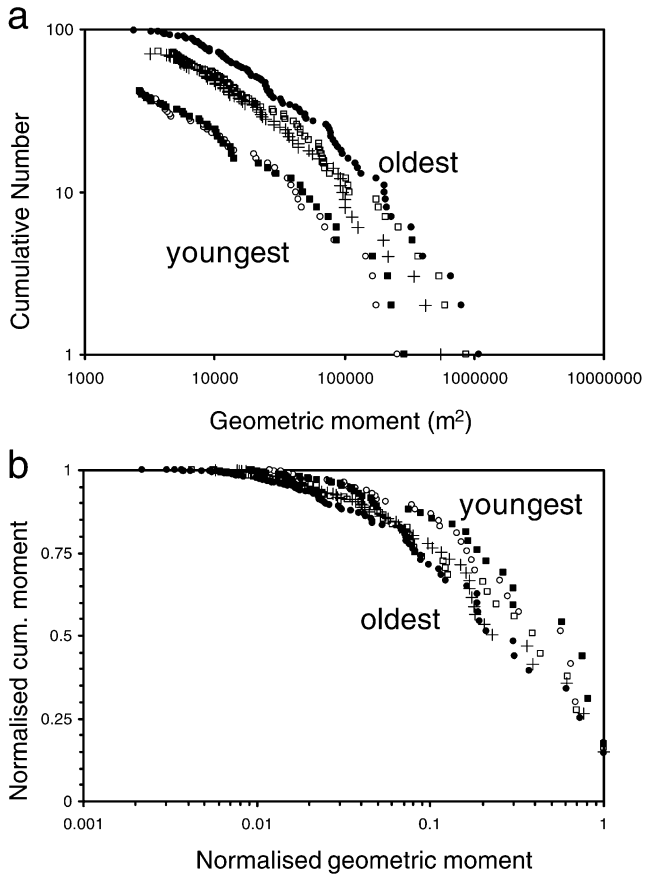

Fig. 11. (a) Cumulative frequency curves of geometric moment for the five syn-faulting horizons A–E. (b) Plot of geometric moment normalised to that of the largest fault on an horizon versus the cumulative moment normalised to the total moment on the same horizon. The horizon datapoint symbols are the same as those in Fig. 6.

moment relates directly to seismic moment (Scholz and Cowie, 1990) facilitating comparison between fault and earthquake populations. The data presented in Fig. 11 have been calculated by integrating the area under the throw profile for each fault and each horizon. The data were modified to correct for truncation of trace lengths by incorporating additional moment at fault tips calculated from a 220 m extension of each fault tip with an average throw of 5 m. Cumulative frequency curves of geometric moment are characteristically convex upwards with up-sequence decreases in the maximum moment and in the total number of faults. These populations are characterised by approximately straight segments for moments between 10^4 and 10^5 m^2, with slopes that decrease slightly up-sequence (Fig. 11a). The curves for the younger horizons have a distinct step at high geometric moments while the older horizons are characterised by a continuous curve. The significance of these changes in curve shape in terms of the distribution of moment, and therefore strain, are best illustrated by a curve of normalised geometric moment against cumulative moment (Fig. 11b). The systematic variations in curve shape with horizon age indicate a progressive change in the distribution of geometric moment with fault size through time where an increasing proportion of the geometric moment is accommodated on the larger faults at later times (e.g. for Horizon E ca.55% of the total geometric moment occurs on faults with normalised geometric moment greater than 0.6 while this value is only 35% for Horizon A). Extrapolating this trend to strains higher than those in the study area, we expect that the continuation of this process of concentration of geometric moments would ultimately result in all of the geometric moment occurring on one or a few dominant faults. This evolution of the active fault population is equivalent to an evolution from a Gutenberg–Richter power-law population to a 'characteristic earthquake' type population (Gutenberg and Richter, 1944; Kanamari and Anderson, 1975), in which the geometric moment of the fault population occurs overwhelmingly on a single or a small number of large structures. Strain localisation onto fewer and larger faults from a more spatially distributed fault array has been observed elsewhere (Nicol et al., 1997; Walsh et al., 2001) and localisation onto a few large faults has been observed in numerical models of fault populations (Cowie et al., 1993; Cowie, 1998).

4. Maximum displacement–fault length relationships

The relationship between maximum displacement (D) and maximum dimension (L) of faults is generally described as a power-law (i.e. $D \propto L^n$) where the exponent, n, ranges from 1 to 2 (e.g. Marrett and Allmendinger, 1991; Cowie and Scholz, 1992; Gillespie et al., 1992; Walsh and Watterson 1992; Dawers et al., 1993; Schlische et al., 1996). The displacement versus length relationship of each syn-faulting horizon has been determined by double regression performed on scatter plots of the raw data (Table 2). However, because of the difficulty of assigning slopes to scatter plots with limited scale ranges (Gillespie et al., 1992), comparison of the slopes of well defined power-law maximum throw and fault trace length populations provides a potentially more robust method for determining the D vs. L relationship which can be described in the form:

$$E_L/E_D = n$$

where E_L is the slope of the length population and E_D the slope of the maximum displacement population (Marrett and Allmendinger, 1991). Using values of E_L from the length populations, which have been modified to reduce truncation and line sampling artefacts (Table 2), the main horizons provide values for E_L/E_D of 1.04 to 1.79, with lower slopes generally characterising younger horizons. These values are typically lower than those estimated from D vs. L scatter plots (Table 2), which also display

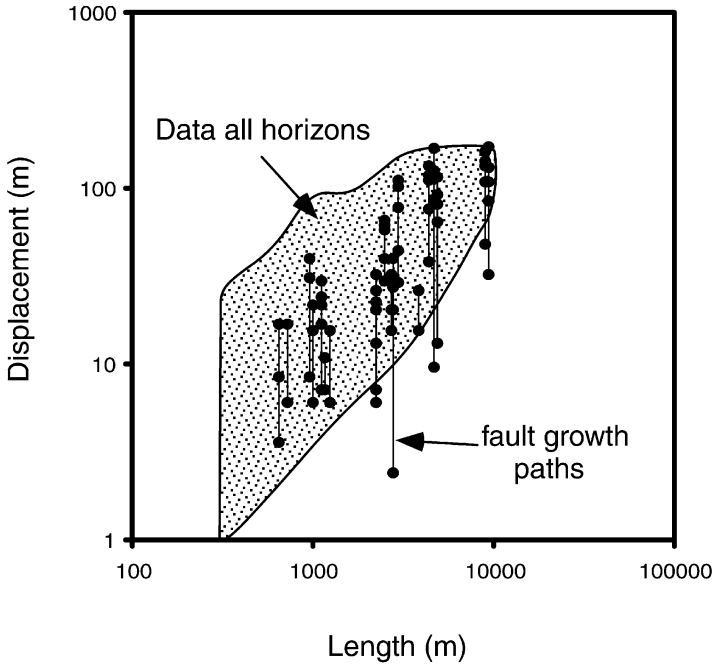

Fig. 12. Displacement vs. length plot showing growth curves for individual faults. The growth curves were calculated by subtracting fault throws on successively older horizons from the throw on Horizon A to determine the length of the fault on Horizon A through time. Calculated in this way the growth curves will show fault propagation where present but not tip-line retreat. The shaded area outlines the distribution of throw vs. length data for all faults on the five syn-faulting horizons.

a general up-sequence decrease in slope. The upward decrease in D vs. L slope is to be expected given that values of E_L decrease upwards within the growth sequence while values of E_D remain approximately constant at -0.85 to -1.15 (Table 2). Factors contributing to up-sequence reduction in the exponent n include decreases in maximum throws, relatively constant fault-trace lengths and reduction in the number of active faults on progressively younger horizons. Upward decreases in fault length and maximum displacement of equal proportions would not produce a significant change in slope. By contrast proportionally larger decreases in displacement as compared with length would result in a decrease in slope. Trace lengths for those faults which offset all five horizons mainly decrease by 10–20% from Horizon A to E (Fig. 3), while maximum displacements decrease by 80–90% (Fig. 4). The significantly higher proportional decrease of displacements, as compared with changes in trace lengths, results in a decrease of slope on upper horizons.

These changes in displacement and length populations reflect changes in the displacements that have accumulated since horizon deposition and do not directly reflect changes in displacement and trace length during fault growth. To examine the D vs. L relationship through time for individual faults, we have backstripped displacements and lengths for 17 faults with a range of maximum throws and lengths. The backstripped data (Fig. 12) show the evolution of displacements and lengths on the A horizon. The backstripping method (Childs et al., 1993) shows the change in length of fault trace on Horizon A through time, rather than the length of the active fault trace at any given time. The curves will therefore show increases in fault length due to propagation, but not decreases in fault length. The curves are approximately parallel to the displacement axis and within the resolution of the data, increases in fault displacement have not been accompanied by increases in fault length. Most faults reached in excess of 80% of their maximum trace length prior to deposition of Horizon B, while these faults had accumulated only 10–30% of their current maximum displacement by this time (e.g. Fig. 8). Therefore, during the first 1–2 my of faulting, trace lengths increased rapidly compared with the maximum displacements, and as a consequence the D vs. L population slopes would have been low compared with those presently observed. Faulting during the last 4 my has been mainly accompanied by an increase in maximum displacement (amounting to 70–90% of current values) with, in some cases, only minor increases in length and in many cases a decrease in fault length. These changes result in a progressive increase in average displacement gradients along the faults which, when coupled with cessation of movement on many of the smaller faults, would be expected to produce an increase in the D vs. L slopes through time at a rate that is controlled in part by the displacement rates.

5. Evolution of the fault population

Formation of the fault population is marked by three broad phases of development; (i) initiation of the fault array, (ii) fault growth and strain concentration and, (iii) death of the fault population. Within the resolution of the data (i) and (ii) occurred under a regime of constant rates of extension while (iii) was associated with a decline in the rates of extension. These stages of fault development overlap in time and are discussed with reference to the times of deposition of the mapped horizons. Therefore, the absolute timing of each stage is regarded as approximate only.

5.1. Initiation of the fault array

This first stage of fault development encompasses the nucleation and early growth of faults to the point where all of the largest faults in the array (e.g. >40 m maximum displacement) were active and the hierarchy of fault sizes established. This period is estimated to span the interval of time between deposition of Horizons A and B. All of the largest faults in the array initiated at, or prior to, deposition of Horizon B within the first 1–2 my of faulting. The timing of onset of displacement varied from fault to fault with the majority of structures (ca. 65%) initiating on the lowermost horizon (A) within the growth sequence (Fig. 4b). Preliminary analysis of fault displacement profiles (e.g. Fig. 8) and maximum displacement vs. length on each horizon (Fig. 12) indicates that many faults reached a significant proportion (70–100%) of their maximum trace lengths during this period of time. This rapid growth of fault length requires that the larger faults propagated laterally at rates in the order of ca. 2–4 km my^{-1}. By contrast, fault-maximum displacements at the base of the growth sequence attained a relatively small proportion (<30%; Fig. 4b) of their current values in the first 1–2 my. Faults at the time of deposition of Horizon B were therefore characterised by long trace lengths and relatively low maximum displacements, which, in combination, produced low lateral displacement gradients. For example, on Horizon A, the fault in Fig. 8a was characterised by average displacement gradients (i.e. length/maximum displacement) of 0.014 at deposition of Horizon B while gradients on this horizon are currently 0.06, a factor of four higher.

Displacement rates of individual faults, which were near-constant through time (Fig. 4b), were also established by about the time of deposition of Horizon B. Given the time resolution of the data, a gradual increase in rates during the early part of this formative stage of faulting, as has been observed in numerical models (Cowie, 1998), cannot be discounted (Nicol et al., 1997). However displacement rates on faults active during this time are comparable with those in later time periods, so that this initial episode of relatively low rates cannot have lasted for long (e.g. ca. <0.5 Ma). Displacement rates were greatest on the largest faults with proportional, rather than absolute, differences in maximum displacements of faults being maintained during evolution of the population (Fig. 4b). The systematic accumulation of displacements within the fault array, together with the rapid development of fault lengths, suggest that the hierarchy of fault sizes was established during nucleation and early growth of the fault system, within a period less than the ca. 1–2 my time resolution. The generation and broad maintenance of a hierarchy of sizes throughout the life of the fault system has been previously attributed to a degree of far-field interaction between the faults, which was in place from the very earliest stage of faulting (Nicol et al., 1997; Cowie, 1998).

One explanation for the rapidly established fault lengths and displacement rates is that some of the faults were reactivated during the late Tertiary and inherited their lengths and relative displacements from pre-existing structures. Faults 2 and 4 (Figs. 3 and 4), two of the largest faults in the population, link with large faults (throw ca.500 m) at the Top Permian level and are interpreted to be reactivated Late Jurassic–Early Cretaceous faults. Localisation of strain onto these faults may have been enhanced by the presence of a pre-existing structure (Fig. 2a). Of the remaining faults, many are confined to the Cenozoic sequence and do not root in Mesozoic structures, but the poor quality of seismic data in the Mesozoic sequence makes it difficult to be certain which faults in these strata are reactivated. Therefore, while the location and geometry of the central graben is strongly influenced by the presence of pre-existing faults, the dimensions and displacements of the majority of faults cannot be directly attributed to reactivation but nor can this be ruled out.

5.2. Fault growth and onset of strain localisation

The second stage of fault growth was associated with an approximately constant extension rate of 0.84% my^{-1} and the onset of strain localisation onto the larger faults. This period of faulting spanned mainly the interval of time between Horizons B and C and is marked by a dramatic slowing in the lateral propagation of fault tips, with extension accommodated principally by increases in displacement. Fault lengths increased by no more than 10–15% (e.g. left tip of Fig. 8a) and in some cases decreased slightly by 5–10% (e.g. Fig. 8b and right tip of Fig. 8a). This decrease in fault tip propagation rate is believed to reflect the onset of local elastic interactions between the tips of propagating faults and are reflected in high displacement gradients approaching the tips of these faults (Nicol et al., 1996). In contrast to the decrease in the rates of lateral propagation, displacement rates were unchanged with on average ca. 20–30% of the total maximum displacement being accommodated on faults during this interval of time. Consequently, the relationships between maximum displacement and fault-trace length began to change significantly, with a substantial decrease in the ratio of fault lengths to maximum displacements and a corresponding

increase in the average displacement gradients. For example, on Horizon A the fault in Fig. 8a was characterised by an average displacement gradient of ca. 0.036 (i.e. *L*:*D* ratio ca. 28) at the time of deposition of Horizon C, considerably higher than the 0.014 gradient at Horizon A time and less than a factor of two lower than the current gradient of 0.06.

The numbers of faults offsetting each horizon decreases above Horizon A (Table 1; Fig. 6). Approximately 15% of faults active at Horizon B ceased to accrue displacement prior to deposition of Horizon C; one such fault is contained in Fig. 4b (number 18) while several others die immediately above Horizon C (numbers 8, 16–18). The smaller faults (e.g. <30 m maximum displacement) within the population generally became inactive earlier than larger faults. The relatively high mortality rates of the smaller faults reduced the total number of faults active in the population and, as rates of extension remained approximately constant over this period (Fig. 5), must have increased the relative proportion of extension accommodated by the larger faults. The increased extension on the large faults could occur by increasing either the lengths or displacement rates of the active faults. The decreased geometric moment due to the death of small faults during this phase of fault system growth, can be balanced by a 1% my^{-1} increase in either the displacement rate or length of the remaining active faults. These changes are below the resolution of the data and the distinction cannot be made.

The progressive concentration of strain on the larger faults can be observed in a qualitative manner from Fig. 3 and is also born out in the fault-size populations (Figs. 7, 9 and 11). It is important to note that this process commenced relatively early in the development of the system but appears to have been accelerated by a decrease in the rates of extension at later times.

5.3. Death of the fault population

The demise of the fault population is marked by a significant decrease (ca. 50–80%) in the rate of extension (Table 1; Fig. 5). This phase of deformation is marked by high mortality rates of faults and by a reduction of active trace lengths (Fig. 8b). The death rate of faults increased by a factor of three after deposition of Horizon C, from seven faults per my between Horizons B and C to 21 faults per my between C and E. As was the case during the previous stage of faulting, the smallest faults within the active fault population had the highest probability of becoming inactive. For those faults which displace Horizon C, for example, only ca. 15% with trace lengths over 2 km became inactive by the time Horizon E was deposited; this number increases to 50% for faults <2 km and 75% for trace lengths <1 km. By contrast, no faults with throws $\geqq$ 30 m on Horizon C became inactive by Horizon E while 50% with throws <30 m died. These statistics illustrate that while fault size is an important factor in determining which faults become inactive, there are other contributing factors. Inspection of Fig. 3a and b suggests that faults destined to die before deposition of the overlying horizon are often clustered (Fault C), and in many cases are located next to a large fault (Fault 4). From this it seems that location also influences fault life expectancy and that faults located adjacent to larger faults may be deprived of extension as the strain shadows of the larger faults grow (e.g. Ackermann and Schlische, 1997; Walsh et al., 2001a). Whatever the mechanism of fault death, the end result is that strain is concentrated onto the larger faults at the expense of the smaller faults in the population.

A critical question remains regarding whether fault death is essentially instantaneous (i.e. fault displacements and active lengths are maintained throughout the life of a fault) or whether faults die slowly by a gradual reduction of displacement rates and active fault lengths. Within the resolution of our dataset there are no indications that maximum displacement rates decrease immediately prior to cessation of movement (Fig. 4b). Indeed the overall impression is that, to a first order, displacement rates do not change as a fault approaches the end of its activity. By contrast, decrease in trace lengths occurred on many of the faults in the dataset (indicated in blue in Fig. 3). Retreat of fault tips was a feature of fault evolution since the early stages of faulting but the proportion of reduced fault length (blue in Fig. 3) to total fault length (black, blue and red traces in Fig. 3) on a given horizon increases post deposition of Horizon C. Retreat may occur on one or both tips and at any one tip commonly accounts for a c. 5–30% decrease in trace length (e.g. fault in Fig. 8a). Decrease in trace length can occur at trace overlaps where the faults are interacting and have dependent displacements (e.g. Fig. 8b). In such cases reduction in trace length may be part of a localisation process where the fault will eventually form a single through-going structure. In the extreme, when a fault population has reached full maturity, incremental extension would be accommodated by a single large fault.

6. Discussion

Fault lengths within the study area were established early (1–2 my) during extension of the basin and later extension was largely accommodated by amplification of displacements on these structures with minimal fault propagation. There are few detailed studies of the growth of fault populations with which these findings can be compared and the generality of this conclusion cannot be established. A similar conclusion was reached by Morley (1999) in a study of the early syn-rift sediment distributions in the East African Rift, where the large basin bounding faults developed at the earliest stages of rifting. In a study of fault propagation rates from a number of areas, Childs et al. (2001) found that fault propagation rates tend to decrease with elapsed time since the initiation of faulting. It is possible

that the rapid initial growth in fault length in the Timor Sea study area is due to the reactivation of pre-existing sub-parallel Mesozoic faults and that faulting of a homogeneous basement, if such a thing exists, may be characterised by a more protracted period of fault length generation.

The early establishment of fault lengths has clear implications for the displacement/length relationships of faults. Large fault lengths established at the outset of fault system evolution and at low fault displacements, will result in low average lateral displacement gradients and a low exponent in the $D \propto L^n$ relationship. As fault system evolution progresses, average fault displacement gradients and the exponent n will increase as the rate of fault propagation decreases and displacement continues to accrue on faults of approximately constant length.

Localisation of strain onto progressively fewer faults during evolution of the Timor Sea fault population occurs against the backdrop of a decreasing rate of extension. High rates of fault mortality do however occur before the extension rate begins to decline and we suggest that the observed localisation of strain would occur even with a constant rate of extension. Nicol et al. (1997) have shown that higher strain rate fault systems are characterised by faster moving faults rather than by having more faults than low strain rate systems. A corollary to their results is that reduction in strain rate need not be accompanied by an increased fault mortality rate. In the limit, the observed localisation process will give rise to a single active fault or segmented fault array traversing the entire area. This degree of localisation has not been achieved at the time of deposition of the youngest mapped horizon within the Timor Sea area, but has been observed in a study of fault system development in the North Sea (Walsh et al., 2001).

The primary evolutionary trend observed for the Timor Sea area is in the progressive and systematic decrease in the slope of the length populations. The slope of the throw populations remained approximately constant through time and is consistent with the approximately constant displacement rates observed in individual faults. In their study of an area of the North Sea, Walsh et al. (2001) observed significant changes in the character of throw populations through time, where one large continuous fault array extends across the entire study area and accrues displacements much larger than would be predicted from the power-law size relationship of the smaller faults. Within the Timor Sea study area, a single dominant fault or soft-linked fault array has not developed. If this were to occur at higher strains, we expect that the fault throw population would evolve towards a characteristic earthquake-type distribution.

7. Conclusions

1. All of the largest faults in the Timor Sea study area (>30 m maximum displacement) initiated within the first 1–2 my of faulting.
2. Fault lengths were established rapidly during the first 1–2 my of deformation. Fault reactivation may partly explain why fault-trace patterns were formed quickly.
3. Displacement rates of individual faults were near constant through time, with larger faults moving faster than small faults. As displacement rates and fault lengths were both established rapidly, the hierarchy of faults in the array was also established early in the history of faulting.
4. The slopes of maximum throw populations remained approximately constant throughout the growth of the fault system, but fault length population slopes decreased through time. Geometric moment and, therefore, extension became concentrated onto progressively larger faults as the fault population evolved.
5. Relationships between the maximum displacement and fault length changed through time. Initially fault length increased more rapidly than maximum displacement, forming long fault traces with low displacements. Following this initial period, fault propagation rates slowed significantly and continued extension was accommodated mainly by increases in displacement on the existing fault traces.
6. As the population evolved, fewer small faults (<30 m maximum displacement) remained active. High mortality rates for the smaller faults reduced the total number of faults active in the population and increased the relative proportion of extension accommodated on the larger faults.
7. This later stage of strain concentration on the larger faults was associated with a reduction in the length of those active faults remaining in the system. Decreases in the number of faults and in fault lengths may partly reflect a slowing of regional rates of extension.

Acknowledgements

We thank staff of BHP Petroleum for provision of data. The manuscript has benefited from the constructive comments of Tom Manzocchi and other members of the Fault Analysis Group. We are grateful to Phillip Nell for his help with seismic interpretation and Ian Waines for assisting with the data collation. Susannah Anderson-Carr and Elizabeth Sweeney helped to prepare the manuscript. Ben Brooks and Roy Schlische are thanked for their constructive reviews of the manuscript. This research was funded by EU Contract Nos ENV4-CT97-5087 and JOF3-CT97-0036.

References

Ackermann, R.V., Schlische, R.W., 1997. Anticlustering of small normal faults around larger faults. Geology 25, 1127–1130.

Ackermann, R.V., Withjack, M.O., Schlische, R.W., 2000. The geometrical and statistical evolution of normal fault systems: an experimental study

of the effects of mechanical layer thickness on scaling laws. Journal of Structural Geology 23, 1803–1819.

Anders, M.H., Schlische, R.W., 1994. Overlapping faults, intrabasin highs and the growth of normal faults. Journal of Geology 102, 165–180.

Cartwright, J.A., Trudgill, B., Mansfield, C.S., 1995. Fault growth by segment linkage: an explanation for scatter in maximum displacement and trace length data from Canyonlands Grabens of S.E. Utah. Journal of Structural Geology 17, 1319–1326.

Childs, C., Walsh, J.J., Watterson, J., 1990. A method for estimation of the density of fault displacements below the limits of seismic resolution in reservoir formations. In: Buller, A.T., Berg, E., Hjelmeland, O., Kleppe, J., Torsaeter, O., Aasen, J.O. (Eds.). North Sea Oil and Gas Reservoirs II. Graham and Trotman, London, pp. 309–318.

Childs, C., Easton, S.J., Vendeville, B.C., Jackson, M.P.A., Lin, S.T., Walsh, J.J., Watterson, J., 1993. Kinematic analysis of faults in a physical model of growth faulting above a viscous salt analogue. Tectonophysics 228, 313–329.

Childs, C., Watterson, J., Walsh, J.J., 1995. Fault overlap zones within developing normal fault systems. Journal of the Geological Society, London 152, 535–549.

Childs, C., Nicol, A., Walsh, J.J., Watterson, J., 2001. The growth and propagation of syn-sedimentary faults. Journal of Structural Geology, in press.

Clausen, O.R., Korstgård, J.A., Petersen, K., McCann, T., O'Reilly, B.M., Shannon, P., Howard, C., Mason, Ph., Walsh, J.J., Watterson, J., 1994. Systematics of faults and fault arrays. In: Helbig, K. (Ed.). Modeling the Earth for Oil Exploration. Final report of the CEC's Geoscience Program 1990–1993, pp. 205–316.

Clifton, A.E., Schlische, R.W., Withjack, M.O., Ackermann, R.V., 2000. Influence of rift obliquity on fault-population systematics: results of clay modelling experiments. Journal of Structural Geology 22 (10), 1491–1509.

Cowie, P.A., 1998. A healing–reloading feedback control on the growth rate of seismogenic faults. Journal of Structural Geology 20, 1075–1087.

Cowie, P.A., Scholz, C.H., 1992. Growth of faults by accumulation of seismic slip. Journal of Geophysical Research 97, 11085–11095.

Cowie, P.A., Vanneste, C., Sornette, D., 1993. Statistical physics model for the spatiotemporal evolution of faults. Journal of Geophysical Research 98 (B12), 21809–21821.

Dawers, N.H., Anders, M.H., 1995. Displacement-length scaling and fault linkage. Journal of Structural Geology 17, 607–614.

Dawers, N.H., Anders, M.H., Scholz, C.H., 1993. Fault length and displacement: scaling laws. Geology 21, 1107–1110.

Ferrill, D.A., Stamatakos, J.A., Sims, D., 1999. Normal fault corrugation: implications for growth and seismicity of active normal faults. Journal of Structural Geology 21, 1027–1038.

Gillespie, P.A., Walsh, J.J., Watterson, J., 1992. Limitations of dimension and displacement data from single faults and the consequences for data analysis and interpretation. Journal of Structural Geology 14, 1157–1172.

Gupta, A., Scholz, C.H., 2000. A model of normal fault interaction based on observations and theory. Journal of Structural Geology 22 (7), 865–879.

Gutenberg, B., Richter, C., 1944. Frequency of earthquakes in California. Bulletin of the Seismological Society of America 34, 185–188.

Heffer, K.J., Bevan, T.G., 1990. Scaling relationships in natural fractures — data, theory and applications. Society of Petroleum Engineers Journal, Paper No. 20981.

Kanamari, H., Anderson, D.L., 1975. Theoretical basis of some empirical relations in seismology. Bulletin of the Seismological Society of America 65, 1073–1095.

Marchal, D., Guiraud, M., Rives, T., Van Den Driessche, J., 1998. Space and time propogation processes of normal faults. In: Jones, G., Fisher, Q.J., Knipe, R.J. (Eds.). Faulting, Fault Sealing and Fluid Flow in Hydrocarbon Reservoirs. Geological Society, London, pp. 51–70.

Marrett, R., Allmendinger, R.W., 1990. Kinematic analysis of fault slip data. Journal of Structural Geology 12, 973–986.

Marrett, R., Allmendinger, R.W., 1991. Estimates of strain due to brittle faulting: sampling of fault populations. Journal of Structural Geology 13, 735–738.

Marrett, R., Allmendinger, R.W., 1992. Amount of extension on 'small' faults: an example from the Viking Graben. Geology 20, 47–50.

McClay, K.R., 1990. Extensional fault systems in sedimentary basins: a review of analogue model studies. Marine and Petroleum Geology 7, 206–233.

Meyer, V., 1997. Champ de failles et deformation globale; approche experimentale et numerique. Application au Nord Ouest de l'Argentine. Publ. PhD Rennes I, France.

Morley, C.K., 1999. Patterns of displacement along large normal faults: Implications for basin evolution and fault propagation, based on examples from East Africa. Bulletin of the American Association of Petroleum Geologists 83, 613–634.

Nicol, A., Walsh, J.J., Watterson, J., Childs, C., 1996. The shapes, major axis orientations and displacement patterns of fault surfaces. Journal of Structural Geology 18, 235–248.

Nicol, A., Walsh, J.J., Watterson, J., Underhill, J.R., 1997. Displacement rates of normal faults. Nature 390, 157–159.

O'Brien, G.W., Higgins, R., 1996. Basement control on the development of extensional systems in Australia's Timor Sea: an example of hybrid hard linked/soft linked faulting? Australian Petroleum Exploration Association Journal 27, 138–158.

O'Brien, G.W., Etheridge, M.A., Willcox, J.B., Morse, M., Symonds, P., Norman, C., Needham, D.J., 1993. The structural architecture of the Timor Sea, north-western Australia: implications for basin development and hydrocarbon exploration. Australian Petroleum Exploration Association Journal 33, 258–278.

Pattillo, J., Nicholls, P.J., 1990. A tectono-Stratigraphic framework for the Vulcan Graben. Timor Sea region. Australian Petroleum Exploration Association Journal 30, 27–51.

Peacock, D.C.P., Sanderson, D.J., 1994. Geometry and development of relay ramps in normal fault systems. Bulletin of the American Association of Petroleum Geology 78, 147–165.

Schlische, R.W., Young, S.S., Ackermann, R.V., Gupta, A., 1996. Geometry and scaling relations of a population of very small rift-related normal faults. Geology 24, 683–686.

Scholz, C.H., Cowie, P.A., 1990. Determination of total strain from faulting using slip measurements. Nature 346, 837–839.

Walsh, J.J., Watterson, J., 1988. Analysis of the relationship between the displacements and dimensions of faults. Journal of Structural Geology 10, 239–247.

Walsh, J.J., Watterson, J., 1989. Displacement gradients on fault surfaces. Journal of Structural Geology 11 (3), 307–316.

Walsh, J.J., Watterson, J., 1991. Geometric and kinematic coherence and scale effects in normal fault systems. In: Roberts, A.M., Yielding, G., Freeman, B. (Eds.). Special Publication of the Geological Society of London, 59, 193–203.

Walsh, J.J., Watterson, J., 1992. Populations of faults and fault displacements and their effects on estimates of fault-related regional extension. Journal of Structural Geology 14, 701–712.

Walsh, J.J., Watterson, J., Childs, C., Nicol, A., 1996. Ductile strain effects in the analysis of seismic interpretations of normal fault systems. In: Buchanan, P.G., Nieuwland, D.A. (Eds.). Modern Developments in Structural Interpretation, Validation and Modelling, Special Publication of the Geological Society of London 99, 27–40.

Walsh, J.J., Childs, C., Meyer, V., Manzocchi, T., Imber, J., Nicol, A., Tuckwell, G., Bailey, W.R., Bonson, C.G., Watterson, J., Nell, P.A.R., Strand, J., 2001. Geometrical controls on the evolution of normal fault systems. In: Holdsworth, R.E. (Ed.). The Nature of the Tectonic Significance of Fault Zone Weakening. Special Publication of the Geological Society of London, 186, 157–170.

Walsh, J.J., Watterson, J., Yielding, G., 1991. The importance of small-scale faulting in regional extension. Nature 351, 391–393.

Watterson, J., 1986. Fault dimensions, displacements and growth. Pure and Applied Geophysics 124, 365–373.

Watterson, J., Walsh, J.J., Gillespie, P.A., Easton, S., 1996. Scaling systematics of fault sizes on large scale range of fault map. Journal of Structural Geology 18, 199–214.

Woods, E.P., 1992. Vulcan Sub-basin fault styles — implications for hydrocarbon migration and entrapment. Australian Petroleum Exploration Association Journal 32, 138–158.

Wormald, G.B., 1988. The geology of the Challis oilfield, Timor Sea, Australia. In: Purcell, P.G., Purcell, R.R., (Eds.), The North West Shelf, Australia, Petroleum Exploration Society of Australia 1988, 425–437.

Yielding, G., Walsh, J.J., Watterson, J., 1992. The prediction of small-scale faulting in reservoirs. First Break 10, 449–460.

Yielding, G., Needham, T., Jones, H., 1996. Sampling of fault populations using sub-seismic data: a review. Journal of Structural Geology 18, 135–146.